



CrossMark

Original Investigation

Using Hyperpolarized ^{129}Xe MRI to Quantify the Pulmonary Ventilation Distribution

Mu He, MS, Bastiaan Driehuys, PhD, Loretta G. Que, MD, Yuh-Chin T. Huang, MD, MHS

Rationale and Objectives: Ventilation heterogeneity is impossible to detect with spirometry. Alternatively, pulmonary ventilation can be imaged three-dimensionally using inhaled ^{129}Xe magnetic resonance imaging (MRI). To date, such images have been quantified primarily based on ventilation defects. Here, we introduce a robust means to transform ^{129}Xe MRI scans such that the underlying ventilation distribution and its heterogeneity can be quantified.

Materials and Methods: Quantitative ^{129}Xe ventilation MRI was conducted in 12 younger (24.7 ± 5.2 years) and 10 older (62.2 ± 7.2 years) healthy individuals, as well as in 9 younger (25.9 ± 6.4 yrs) and 10 older (63.2 ± 6.1 years) asthmatics. The younger healthy population was used to establish a reference ventilation distribution and thresholds for six intensity bins. These bins were used to display and quantify the ventilation defect region (VDR), the low ventilation region (LVR), and the high ventilation region (HVR).

Results: The ventilation distribution in young subjects was roughly Gaussian with a mean and standard deviation of 0.52 ± 0.18 , resulting in $\text{VDR} = 2.1 \pm 1.3\%$, $\text{LVR} = 15.6 \pm 5.4\%$, and $\text{HVR} = 17.4 \pm 3.1\%$. Older healthy volunteers exhibited a significantly right-skewed distribution (0.46 ± 0.20 , $P = 0.034$), resulting in significantly increased VDR ($7.0 \pm 4.8\%$, $P = 0.008$) and LVR ($24.5 \pm 11.5\%$, $P = 0.025$). In the asthmatics, VDR and LVR increased in the older population, and HVR was significantly reduced ($13.5 \pm 4.6\%$ vs $18.9 \pm 4.5\%$, $P = 0.009$). Quantitative ^{129}Xe MRI also revealed altered ventilation heterogeneity in response to albuterol in two asthmatics with normal spirometry.

Conclusions: Quantitative ^{129}Xe MRI provides a robust and objective means to display and quantify the pulmonary ventilation distribution, even in subjects who have airway function impairment not appreciated by spirometry.

Key Words: Asthma; aging; albuterol.

© 2016 The Association of University Radiologists. Published by Elsevier Inc. All rights reserved.

INTRODUCTION

The distribution of ventilation is known to be nonuniform in healthy lungs (1–6), and this heterogeneity increases with age and disease. Ventilation heterogeneity is impossible to quantify using spirometry because it measures the lung as a single unit and is insensitive to pathology in the small airways—the so-called silent zone. Alternative approaches include using the multiple-breath

nitrogen washout (MBNW) test to determine the distribution of specific ventilation (SV) (2,7), the lung clearance index (LCI) (8–11), or the multiple inert gas elimination technique (MIGET) to quantify the ventilation–perfusion relationship (6); however, none of these tests provides spatial information. Alternatively, imaging methods such as computed tomography (CT) delineate spatial changes in lung structures that may allow ventilation abnormalities to be inferred. However, CT does not directly measure ventilation and its radiation dose limits some longitudinal studies.

Recently, magnetic resonance imaging (MRI) techniques have emerged that enable direct detection of inhaled gases, such as oxygen (12–14), perfluorinated gases (15,16), and hyperpolarized (HP) ^3He (4,17,18). These techniques enable visualization of ventilation defects that have been shown to correlate with airway tone (4,19–21) and airway abnormalities (22). HP ^3He MRI readily depicts regional ventilation heterogeneity in patients with pulmonary obstructive diseases (23). More recently, ^{129}Xe gas has emerged as the most promising alternative to address dwindling supplies of ^3He (24–26). ^{129}Xe MRI appears to more readily detect ventilation defects than ^3He MRI (21,27) and has been used to visualize elimination of ventilation defects after bronchodilator administration (28).

Acad Radiol 2016; 23:1521–1531

From the Center for In Vivo Microscopy, Duke University Medical Center (M.H., B.D.); Department of Electrical and Computer Engineering, Duke University (M.H.); Department of Biomedical Engineering, Duke University (B.D.); Department of Radiology, Duke University Medical Center, Durham, North Carolina (B.D.); Department of Medicine, Duke University Medical Center, 1821 Hillandale Road, Suite 25A, Durham, NC 27710 (L.G.Q., Y.-C.T.H.). Received April 13, 2016; revised June 22, 2016; accepted July 15, 2016. Authors' contributions: All authors designed the method in this study. M.H. and Y.T.H. performed the statistical analysis. All authors interpreted the data, prepared the manuscript, and drafted the article. All authors approved this manuscript in its final form. Funding support: This study was supported by The Duke Private Diagnostic Clinic Enhanced Academics in a Basic Laboratory Environment (ENABLE) Award (R01HL105643, R01HL126771, P41 EB015897). Address correspondence to: Y.-C.T.H. e-mail: huang002@mc.duke.edu

© 2016 The Association of University Radiologists. Published by Elsevier Inc. All rights reserved.
<http://dx.doi.org/10.1016/j.acra.2016.07.014>

However, the analysis of ^{129}Xe MRI scans has yet to fully capture the entire pulmonary ventilation distribution. Most methods have focused on quantifying the ventilation defect percentage (VDP), the fraction of the lung with ventilation below an arbitrary threshold (29, 31). Although VDP quantifies the most severely affected lung units, its definition is not robust. Moreover, VDP does not report on lung units with mild to moderate impairment or increased ventilation. This finding has led to efforts to extend beyond the VDP, including heterogeneity (4,25,28). Recently, more sophisticated methods such as the hierarchical k -means clustering algorithm have been introduced (30) to derive five different ventilation levels from ^3He MRI and these levels were quantified in asthmatics (32). For ^{129}Xe MRI, our own group has recently introduced a method to rescale image intensity into four bins (31) and has shown VDP derived from such maps to be reproducible to $\pm 1.52\%$ (33). However, it has not yet been determined how these maps could be used to recover the pulmonary ventilation distribution.

Here, we present a novel approach to analyzing ^{129}Xe MRI scans that combines image histogram characterization and linear binning maps to more comprehensively map and quantify the underlying distribution of pulmonary ventilation. We illustrate its utility by detecting abnormalities in the scans from older normal subjects with normal spirometry. We subsequently characterize ventilation distribution differences in older and younger asthmatics, and illustrate the way in which it is altered by bronchodilator therapy.

METHODS

Subjects

We recruited 12 healthy young (18–30 years old) and 10 healthy older (50–70 years old) individuals who were non-smokers, with $\text{FEV}_1 > 85\%$ according to ethnically appropriate reference tables and $\text{FEV}_1/\text{FVC} > 0.7$. We also recruited 9 younger (18–30 years old) and 10 older (50–70 years old) patients with mild intermittent asthma. Each subject provided informed consent to participate in the study protocol.

Image Acquisition

All magnetic resonance (MR) scans were performed on a 1.5-T EXCITE 15M4 MR system (GE Healthcare) using protocols described previously (31). Briefly, subjects were fitted in the supine position with a flexible chest coil (Clinical MR Solutions, Brookfield, WI) that was tuned to the 17.66-MHz ^{129}Xe frequency and proton blocked to permit acquisition of anatomical scans using the ^1H body coil. After the initial localizer and thoracic cavity scans (described subsequently), all subjects underwent ^{129}Xe ventilation MRI after inhaling a dose equivalent (DE) of 71 mL HP ^{129}Xe filled to 1 L total volume with helium buffer gas (34). Some asthmatics underwent additional ^{129}Xe ventilation MRI scans after four puffs

of albuterol with lower DE = 24 mL, 10 minutes after the first ^{129}Xe MRI scan. Scan parameters (71 mL/24 mL DE) were fast spoiled gradient echo, field of view = 40/48 cm, matrix = $128 \times (90\text{--}128)/64 \times 64$, slice thickness = 12.5 mm, bandwidth = 8.3 kHz, flip angle = $7^\circ\text{--}10^\circ$, and repetition time/echo time = 8.1/1.9 ms; Slices were acquired in an anterior to posterior order (34). The ^{129}Xe gradient-echo ventilation images were analyzed in the context of a thoracic cavity image acquired of the same slices using a breath-hold ^1H steady-state free precession imaging sequence using the scanner's body coil. For this anatomical reference scan, subjects were in the same position as for ^{129}Xe MRI and inhaled a 1-L bag of room air. The ^1H images were then acquired with field of view = 40 cm, matrix = 192×192 , slice thickness = 12.5 mm, flip angle = 45° , repetition time/echo time = 2.8/1.2 ms, and bandwidth = 125 kHz. All ^1H and ^{129}Xe MR images were reconstructed directly from the scanner and exported as $256 \times 256 \times 14$ DICOM slices for analysis.

Image Analysis

Image analysis employed an extension of the method (31) we previously introduced to transform gray-scale ^{129}Xe MR images into maps that depict various levels of signal intensity. As illustrated in Figure 1, this method overcomes the lack of absolute MR signal scale (unlike Hounsfield units in CT) by analyzing the ^{129}Xe image in the context of a thoracic cavity mask and using the top percentile of intensities to rescale the image histogram to range from 0 to 1. In addition to correcting for the effects of vasculature and ^{129}Xe coil bias field, we applied two additional technical extensions. We now retain signal from the major airways before histogram rescaling, but remove it before quantitative reporting; these airways replenish fully with each breath and contribute the top percentile of intensities. Furthermore, we erode the thoracic cavity mask by 1 pixel to minimize false defects near the lung borders.

To establish an unbiased reference distribution, we first characterized the averaged rescaled ^{129}Xe intensity histograms from healthy young volunteers. Of the 12 younger volunteers scanned, images from 10 were deemed to exhibit no ventilation defects by visual inspection. From these subjects, an averaged rescaled intensity histogram was generated, and the mean and standard deviation (SD) of this histogram were used to define the threshold intensities for the ensuing six-bin maps. The mean of this distribution defined the boundary between bins 3 and 4, which were classified as the normally ventilated regions. Each bin was assigned a width of 1 SD. The lowest intensity bin was identified as the ventilation defect region (VDR), followed by the low ventilation region (LVR), while the highest two bins were combined to form the high ventilation region (HVR). These same definitions were then used to analyze all subsequent images by classifying each pixel into one of the six bins. In addition, the coefficient of variation (CV) of each rescaled distribution was calculated by taking the ratio of its SD to its mean. Each image was then displayed

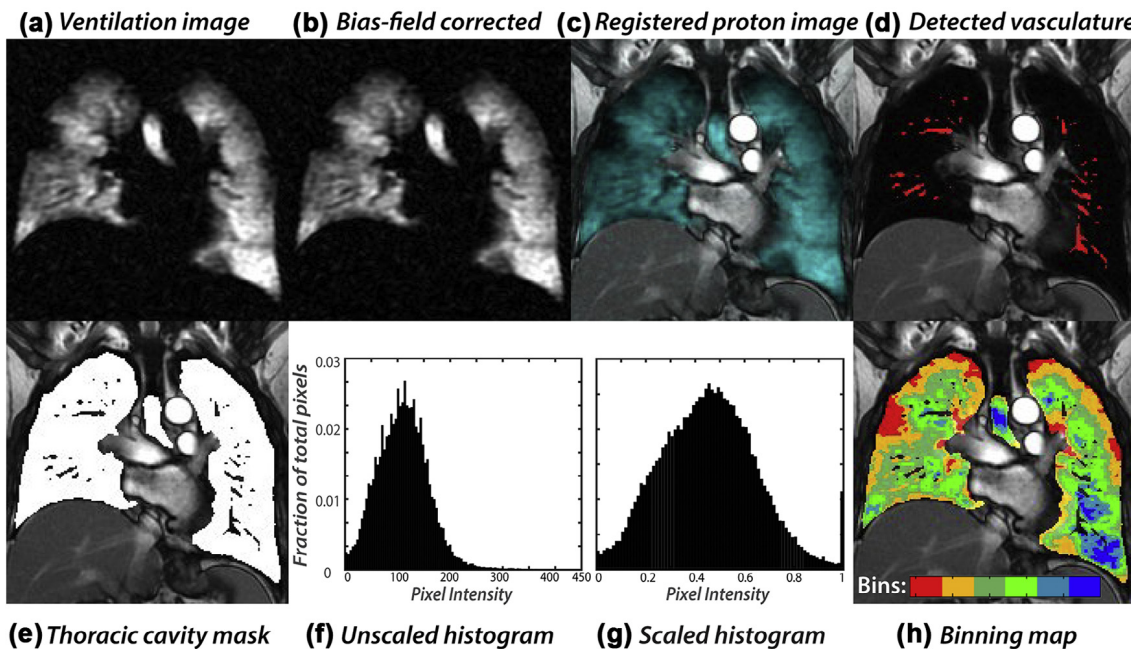


Figure 1. (a) ¹²⁹Xe MRI as acquired. (b) After correction for B1 inhomogeneity. (c) ¹H thoracic cavity image registered to ¹²⁹Xe MRI. (d) Detection of vascular structures within the ¹H image. (e) Segmentation and 1-pixel erosion to create a thoracic cavity mask with vascular structures removed, (f) histogram of ¹²⁹Xe intensities within the mask, and (g) ¹²⁹Xe histogram after rescaling by the top percentile of all intensities. (h) Binning map generated after applying thresholds. MRI, magnetic resonance imaging.

in its original gray scale, as a six-bin color map, and with its associated histogram depicting the rescaled intensity distribution relative to that of the young, healthy reference population.

Statistical Methods

Pulmonary function tests and binning map quantification were tested for significant differences between age and asthmatic groups using a one-tailed Student's *t*-test. This approach was justified given that previous ³He literature had shown that ventilation defects increase and lung function declines as age increases (21). The skewness of the distribution was assessed by Pearson's moment coefficient of skewness. Differences were considered significant when the probability of a type 1 error was 0.05 or less. All statistical analyses were performed using JMP 11 (SAS Institute Inc., Cary, NC).

RESULTS

Study Population

After excluding two healthy subjects with ventilation defects, the study included 10 younger healthy subjects (age: 24.7 ± 5.2 years, FEV1: $103.9 \pm 13.3\%$ predicted), 10 older healthy subjects (age: 62.2 ± 7.2 years, FEV1: $97.7 \pm 13.9\%$ predicted), 9 younger asthmatics (age: 25.9 ± 6.4 years, FEV1: 84.3 ± 16.3 predicted), and 10 older asthmatics (age: 63.2 ± 6.1 years, FEV1: 79.5 ± 22.4 predicted).

Distribution of Ventilation in Young Healthy Subjects

The rescaled ¹²⁹Xe ventilation distributions for each of the healthy young individuals are shown in Figure 2; each exhibited a nearly Gaussian shape and when all 10 were combined, the distribution had a mean of 0.52 and an SD of 0.18. These parameters generated thresholds for the binning maps of 0.16, 0.34, 0.52, 0.70, and 0.88. When these thresholds were applied to the healthy younger subject population, they exhibited volume fractions of VDR = $2.1 \pm 1.3\%$, LVR = $15.6 \pm 5.4\%$, and HVR = $17.4 \pm 3.1\%$. For these young healthy volunteers, the average skewness of the ventilation distribution was 0.0 ± 0.1 and the CV was 0.37 ± 0.04 .

Effects of Age

Figure 3a compares the images, binning maps, and distribution histograms of a 27-year-old healthy subject with FEV1 = 86% (using South Asian reference table (35)) to those of a 58-year-old healthy subject with FEV1 = 102%. The healthy younger subject exhibits a relatively homogenous ventilation distribution with the bulk of the voxels falling within the central green bins and some intensity in the HDR region. The VDR and LVR (red and orange bins) were similar to the reference, and the CV was 0.31. By contrast, the older subject, despite having a normal FEV1, exhibits elevated VDR (9.4%) and LVR (32.2%) visually, as well as an increased CV of 0.50. As shown in Figure 3b, this older control exhibited a right-skewed distribution (skewness = 0.47) histogram relative to the reference population.

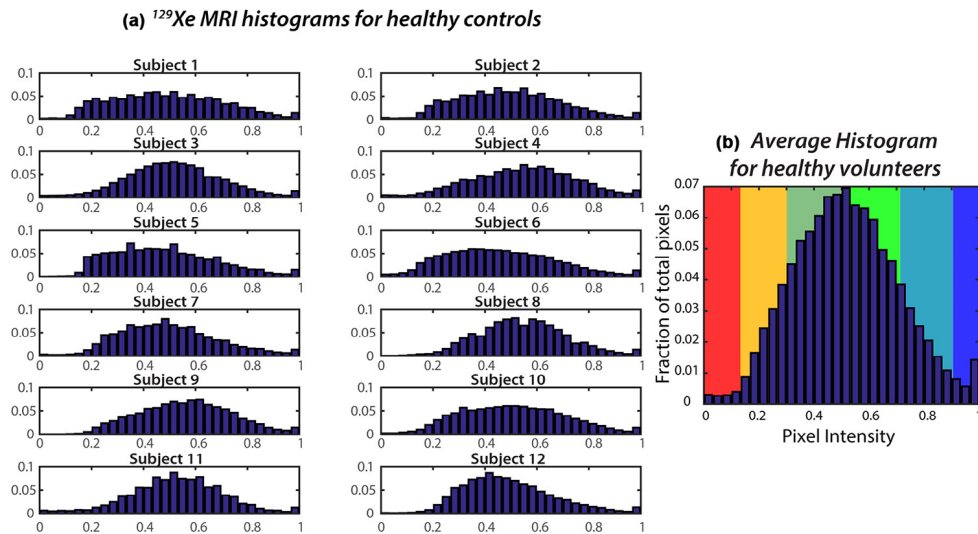


Figure 2. (a) Rescaled ventilation distribution for the 10 young normal individuals. (b) Average distribution for the 10 subjects has a mean of 0.52 and a standard deviation of 0.18. This distribution was used to define the thresholds and widths of six bins used to quantify and map the ventilation distribution.

FEV1 is the maximal amount of air you can forcefully exhale in one second. It is then converted to a percentage of normal

FEV1 greater 80% of predicted = normal
 FEV1 60% to 79% of predicted = Mild obstruction
 FEV1 40% to 59% of predicted = Moderate obstruction
 FEV1 less than 40% of predicted = Severe obstruction

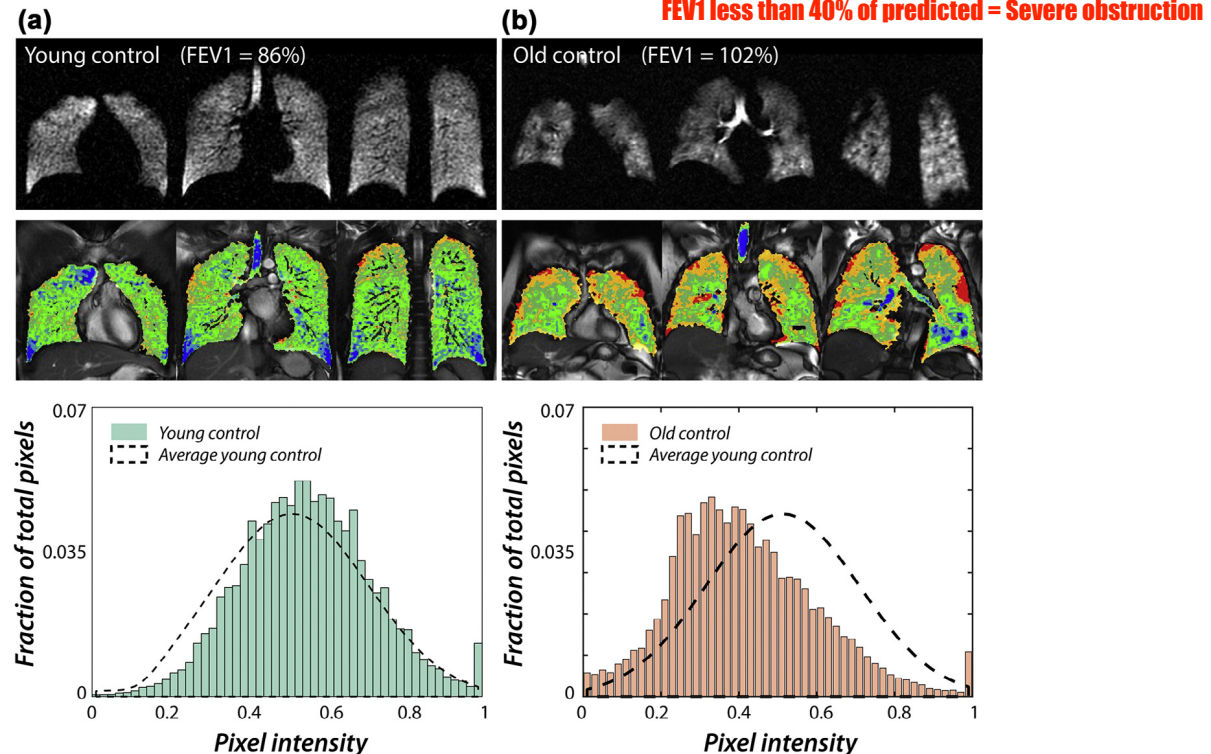


Figure 3. Examples of ^{129}Xe -derived ventilation distributions in a healthy younger and older subject. (a) In a 27-year-old healthy subject with an FEV1 of 86%, the ^{129}Xe ventilation image shows very few ventilation defects. The associated histogram is similar to that of normal young controls, with a mean of 0.54 and an SD of 0.18. (b) In a 58-year-old healthy subject with an FEV1 of 102%, the ventilation image shows areas of ventilation defects (red) and low ventilation (orange). The associated ventilation histogram shifted toward lower values compared to that of normal young controls, with a mean of 0.40 and an SD of 0.20. SD, standard deviation. (Color version of figure is available online.)

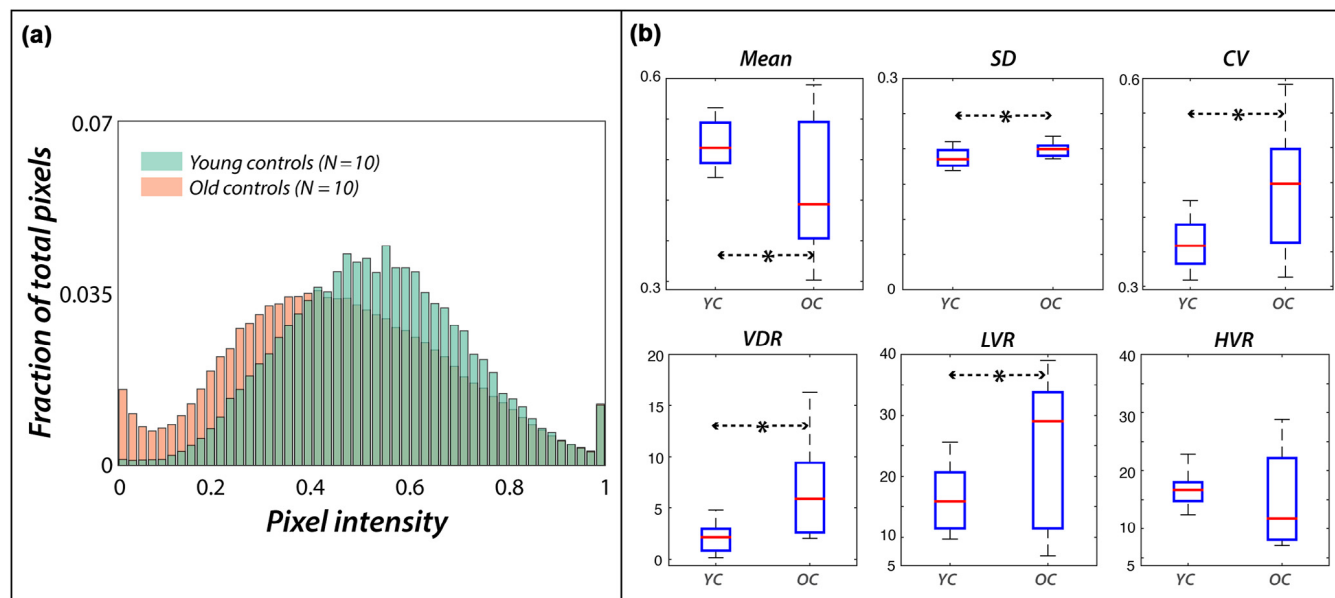


Figure 4. Comparison of ventilation distribution parameters between the YC and OC groups. **(a)** Ventilation distribution histogram from the OC group (red) is overlaid with that from the YC group (blue). The ventilation distribution in the older healthy subjects shifted toward lower values compared to the younger group. **(b)** Comparison of ventilation distribution parameters between the young and old groups shows significant differences for all parameters except HVR (* indicates $P \leq 0.05$). CV, coefficient of variation; HVR, high ventilation region; LVR, low ventilation region; OC, older control; SD, standard deviation; VDR, ventilation defect region; YC, younger control. (Color version of figure is available online.)

As seen in Figure 4, the aggregate ventilation distribution in the older healthy subjects was right skewed (skewness = 0.36) compared to the younger group, resulting in a significantly lower mean value (0.46 ± 0.08 , $P = 0.034$), and a significantly increased SD (0.20 ± 0.01 , $P = 0.017$). As a result, this group exhibited a significantly increased VDR ($7.0 \pm 4.8\%$, $P = 0.0076$) and LVR ($24.5 \pm 11.5\%$, $P = 0.025$) compared to the younger normal reference group. The increased fractions of VDR and LVR appear to have depleted the populations of the two middle bins, whereas HVR remained close to the reference ($14.7 \pm 7.5\%$, $P = 0.20$). In this older population, the higher SD and lower mean of the ventilation distribution also caused heterogeneity to increase, as reflected by a significantly higher CV (0.45 ± 0.09 , $P = 0.014$).

Ventilation Distribution in Older and Younger Asthmatics

Figure 5 shows representative gray-scale images, six-bin maps, and ventilation distribution histograms for a 36-year-old asthmatic with FEV1 = 76% and a 68-year-old asthmatic with FEV1 = 53%. For this example, the younger subject exhibited no significant ventilation defects (VDR = 2.1%) and a relatively high fraction of HVR (24.1%). By contrast, the older asthmatic exhibited more ventilation defects (VDR = 14.0%) and a significantly diminished HVR (9.3%). As shown in Figure 5a, this young asthmatic had a distribution histogram that was similar, and even slightly left skewed (skewness = -0.1), relative to the reference population. By contrast, in the older asthmatic, the histogram was right skewed

(skewness = 0.56), with substantial depletion of the higher-intensity bins (Fig 5b).

Comparison of the younger and older asthmatic groups (Fig 6) reveals not only that VDR ($11.4 \pm 9.4\%$, $P = 0.02$) and LVR ($20.2 \pm 6.7\%$, $P = 0.016$) are increased in the older asthmatics but also that HVR is significantly diminished ($13.5 \pm 4.6\%$, $P = 0.009$). As was the case for older healthy subjects, aging in asthma caused heterogeneity to increase (skewness = 0.06 for younger asthmatics and 0.32 for older asthmatics), resulting in an elevated SD (0.21 ± 0.02 , $P = 0.049$), CV (0.48 ± 0.12 , $P = 0.017$), and a decreased mean (0.45 ± 0.07 , $P = 0.008$) relative to younger asthmatics.

Differences between FEV1 and ¹²⁹Xe MRI Ventilation Distribution

We subsequently used these methods of characterizing the ¹²⁹Xe ventilation distribution to illustrate several individual cases in which ¹²⁹Xe MRI and spirometry convey contrasting pictures of lung function. Shown in Figure 7 are cases of 4 asthmatics—one with normal FEV1 but abnormal ¹²⁹Xe MRI (Fig 7a), one with abnormal FEV1 but normal ¹²⁹Xe MRI (Fig 7b), and two with moderate asthma (Fig 7c and d) who have similarly low FEV1 but radically different ventilation patterns. The 69-year-old asthmatic in Figure 7a had FEV1 = 90% but a ventilation distribution that was right skewed from the reference distribution. This resulted in visible defects and increased VDR (10.4%). By contrast, the 19-year-old asthmatic in Fig 7b had FEV1 = 77% but a ventilation distribution nearly identical to the reference curve. The subjects in Figure 7c

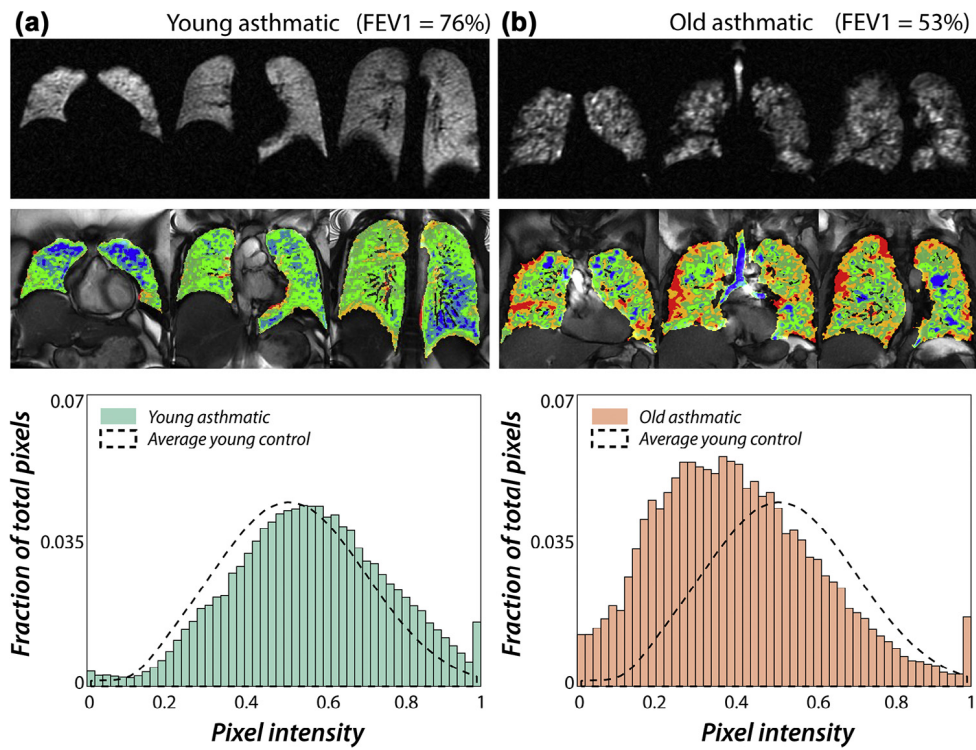


Figure 5. Representative ventilation distributions in a younger asthmatic and an older asthmatic. **(a)** The younger asthmatic with an FEV1 of 76% exhibits a ventilation image with very few ventilation defects. The associated histogram is similar to that of normal young controls. **(b)** The older asthmatic with an FEV1 of 53% has a ventilation image with significant areas of ventilation defects (red) and low ventilation (orange). The associated ventilation histogram of the older asthmatic was significantly right skewed compared to that of the normal young controls. (Color version of figure is available online.)

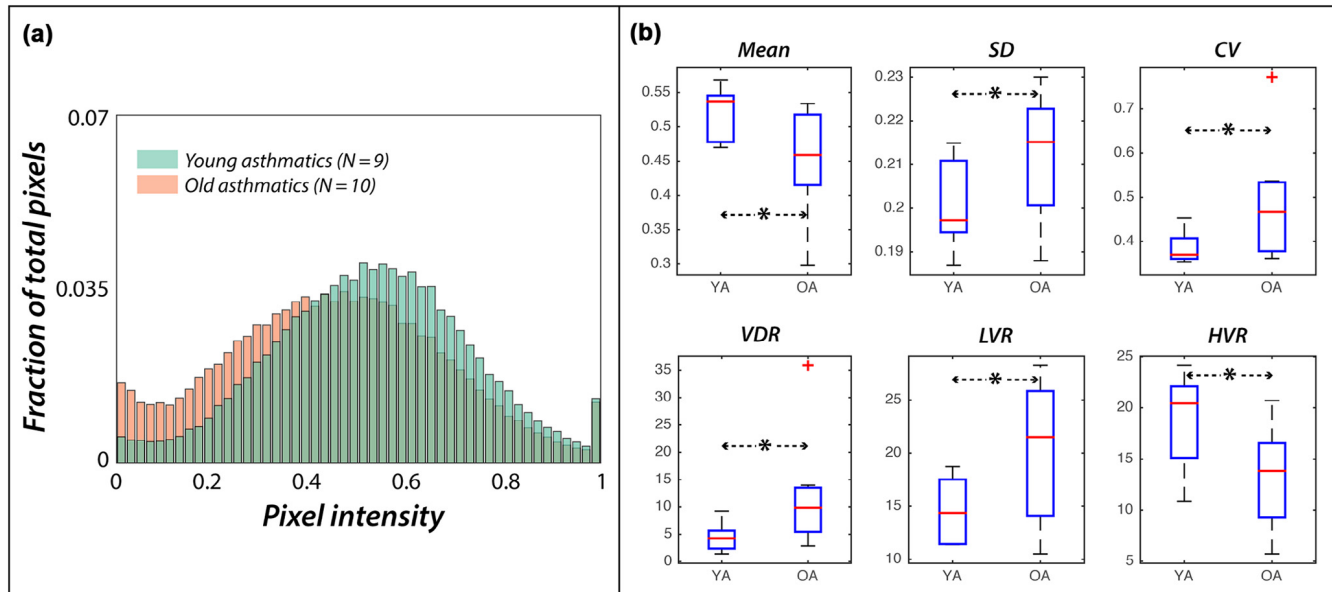


Figure 6. Comparison of ventilation distributions between the YA and OA groups. **(a)** Ventilation distribution histogram from the OA group (red) is overlaid with that from the YA group (blue). In the OA group, the distribution is shifted toward lower values compared to the younger asthmatic group. **(b)** Comparison of ventilation distribution parameters between the YA and the OA groups shows significant differences in all parameters (* indicates $P \leq 0.05$). CV, coefficient of variation; HVR, high ventilation region; LVR, low ventilation region; OA, older asthmatic; SD, standard deviation; VDR, ventilation defect region; YA, younger asthmatic. (Color version of figure is available online.)

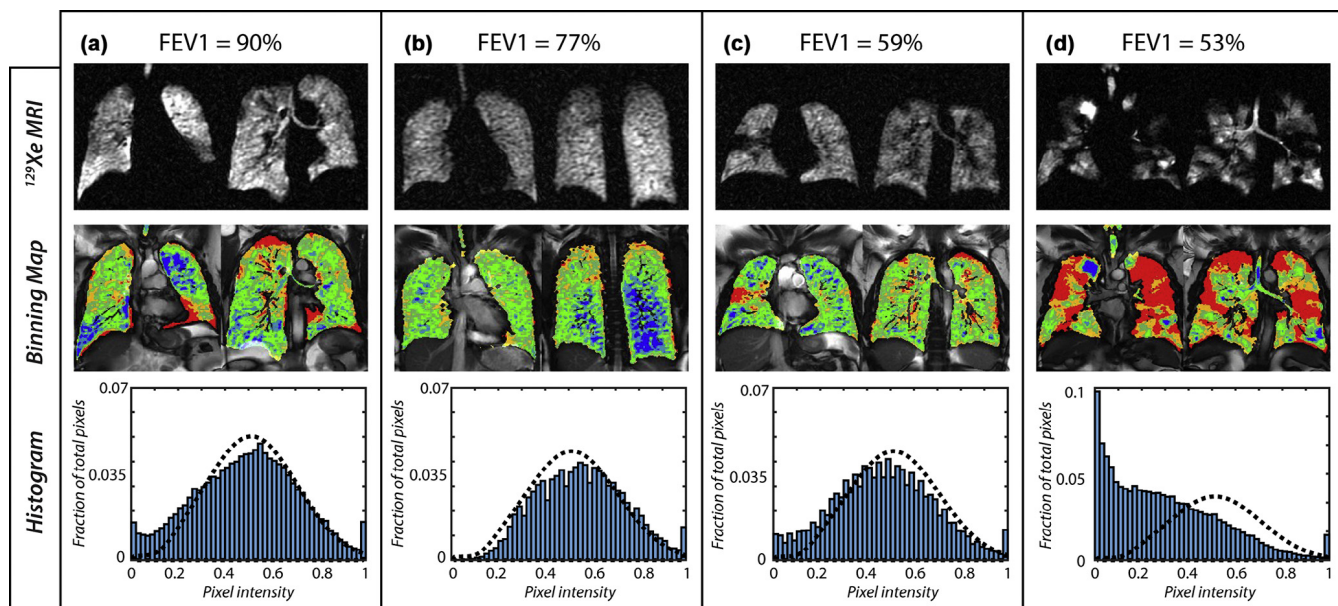


Figure 7. Comparisons between FEV1 and ¹²⁹Xe MRI-derived ventilation distribution in patients with asthma. **(a)** A patient with normal FEV1 but abnormal ¹²⁹Xe MRI. **(b)** A patient with abnormal FEV1 but normal ¹²⁹Xe MRI. **(c and d)** Two patients with moderate asthma with similarly low FEV1 but markedly different ventilation patterns.

and d had similar FEV1s of 59% and 53%; however, the subjects' ventilation distributions bear little resemblance to one another. The subject in Figure 7c exhibited a relatively homogenous ventilation distribution, with the bulk of the voxels falling within the central green bins. This subject exhibited only a slightly elevated VDR (7.9%), whereas the LVR (18.7%) and HVR (15.5%) remained within the normal range. By contrast, the subject in Figure 7d exhibited a greatly elevated VDR (35.9%) and LVR (25.8%) but a significantly diminished HVR (5.7%).

Ventilation Distribution Before and After Albuterol Treatment

Quantitative ¹²⁹Xe MRI can also be used to evaluate bronchodilator response in patients with normal FEV1. Figure 8 shows ¹²⁹Xe MRI and the associated binning analysis in a patient with mild intermittent asthma (FEV1 = 86%) before and after bronchodilator administration. At baseline, the binning map exhibits high percentages of VDR (13.5%) and LVR (27.8%), especially in the right lower lobe, and somewhat lower than normal HVR of 11.5%. After four puffs of albuterol, the patient's FEV1 increased by 15% to a value of 101% predicted (classifying them as a "responder"), and the binning map (Fig 8b) showed a commensurate reduction in both VDR (2.4%) and LVR (15.2%), while HVR increased (17.2%). The associated histogram shifted to higher values and approached the healthy young control distribution. Figure 9 shows a second patient with mild intermittent asthma with FEV1 of 90% predicted before albuterol treatment. For this patient, the binning map at baseline (Fig 9a) exhibited a slightly elevated VDR (6.4%)

and a relatively normal LVR (15.5%) and HVR (18.2%). After albuterol treatment, there was no appreciable change in FEV1 (91% predicted or a "nonresponder"). In this patient, the ¹²⁹Xe VDP decreased somewhat (from 6.4% to 3.2%), but LVR actually increased from 15.5% to 23.4% (Fig 9b). This view is more easily grasped by evaluating the patient's ventilation histograms, which paradoxically shifted toward lower values.

DISCUSSION

Clinical application of ¹²⁹Xe MRI requires accurate quantification and visualization of the ventilation abnormalities. In the present study, we report initial results from a novel ¹²⁹Xe MRI analysis approach that not only accounts for defects but also represents and quantifies the ventilation distribution in its entirety. The essence of the method is to rescale the native ¹²⁹Xe MR image intensities by their top percentile such that the distribution ranges from 0 to 1. Applying such rescaling to the ¹²⁹Xe MRI scans from 10 healthy younger volunteers without visible ventilation defects revealed that the aggregate distribution was nearly Gaussian. From it, a mean and SD could be derived and used to define the thresholds and widths for six bins used to generate quantitative color maps. These maps, in turn, permit both visualization and quantification of the regions containing absent, low, normal, and high ventilation.

This method builds on several previously published HP gas MRI analysis methods. Like those, it readily reports the ventilation defect (20,25,29,31,36), but now replaces subjective thresholds with unbiased ones derived from a well-defined reference population, and reports on the complete ventilation distribution. Moreover, like the hierarchical k-means

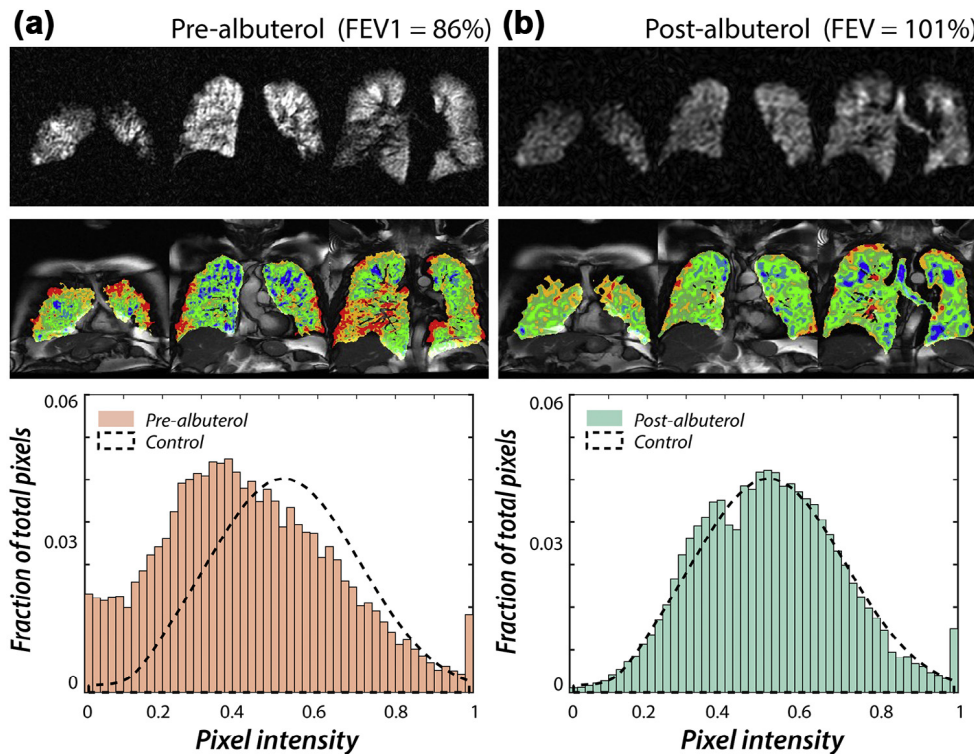


Figure 8. Ventilation distribution in a patient with mild intermittent asthma who had positive bronchodilator response to albuterol based on FEV1 criteria. **(a)** The binning map (top) and histogram (bottom) before albuterol. **(b)** The binning map (top) and histogram (bottom) after albuterol showed a decreased ventilation defect region and low ventilation region, and a distribution matching that of young normal controls after bronchodilator use.

clustering method, our new approach extends the analysis beyond VDP to quantify the remaining aspects of the ventilation distribution (30). However, in our hands, we found the binning approach described here to involve fewer assumptions than *k*-means, which can be affected by the choice of initial centroids and the number of clusters (37). Moreover, the *k*-means may not perform well in the case of unevenly sized or overlapping clusters (38). The binning approach also connects naturally to physiological principles and may therefore be more intuitive to practicing clinicians.

Using the methods outlined here, we found that young healthy individuals exhibit a narrow ventilation distribution. This finding agrees qualitatively with ventilation distributions measured by the MIGET (1), where the differential blood excretion of soluble inert gases is fit to a 50-compartment model. Our approach can also be loosely related to the imaging-derived calculations of fractional ventilation and specific ventilation. Fractional ventilation measures the turnover of gas on a voxel-by-voxel basis and typically requires inhalation or exhalation of multiple breaths (39), a series of image registration steps, and numerous corrections to account for polarization losses (40). Such methods were recently used by Horn et al. with ^3He MRI to estimate fractional ventilation distributions in four healthy subjects and reported $r = 0.25 \pm 0.11$ (41). Similarly, Hamedani et al. recently reported $r = 0.24 \pm 0.06$ for ^3He MRI (42). A closely related measure is SV, which was measured by Sa et al. using oxygen-enhanced proton MRI

in eight healthy individuals, with a mean of $0.24\text{--}0.42$ and an SD of $0.08\text{--}0.14$ (43). Converting these averages to fractional ventilation using $r = \text{SV}/(\text{SV}+1)$ yields $r \sim 0.25 \pm 0.10$. Thus, it appears that the ventilation distribution with a mean of 0.52 ± 0.18 , derived by our relatively simple but robust rescaling approach, can be loosely related to more rigorous and technically challenging multibreath measures of fractional ventilation by a factor of ~ 0.5 .

The six-bin analysis method proved capable of detecting subtle ventilation changes in older individuals who have normal spirometry. Similar age-related changes have been reported using HP ^3He MRI by Sheikh et al., who found ventilation defects in lung periphery in 39 of 52 elderly nonsmokers (44). Such defects can be understood in the context of the aging lung, which undergoes pathological changes, such as degeneration of small airways and loss of tissue support for peripheral airways. These, in turn, lead to increased ventilation heterogeneity and appearance of low ventilation/perfusion (VA/Q) regions (44–46). In our analysis, this finding is reflected in greater fractions of VDR and LVR that can be appreciated and explained by the right skewing of the ventilation distribution in older subjects. Such aging-related effects have also been reported by Cardus et al., who used MIGET to confirm that the log standard deviation of ventilation (log SDv) increases slightly with age (46). These age-specific physiological changes will need to be considered when interpreting ventilation distribution results from ^{129}Xe MRI in older individuals.

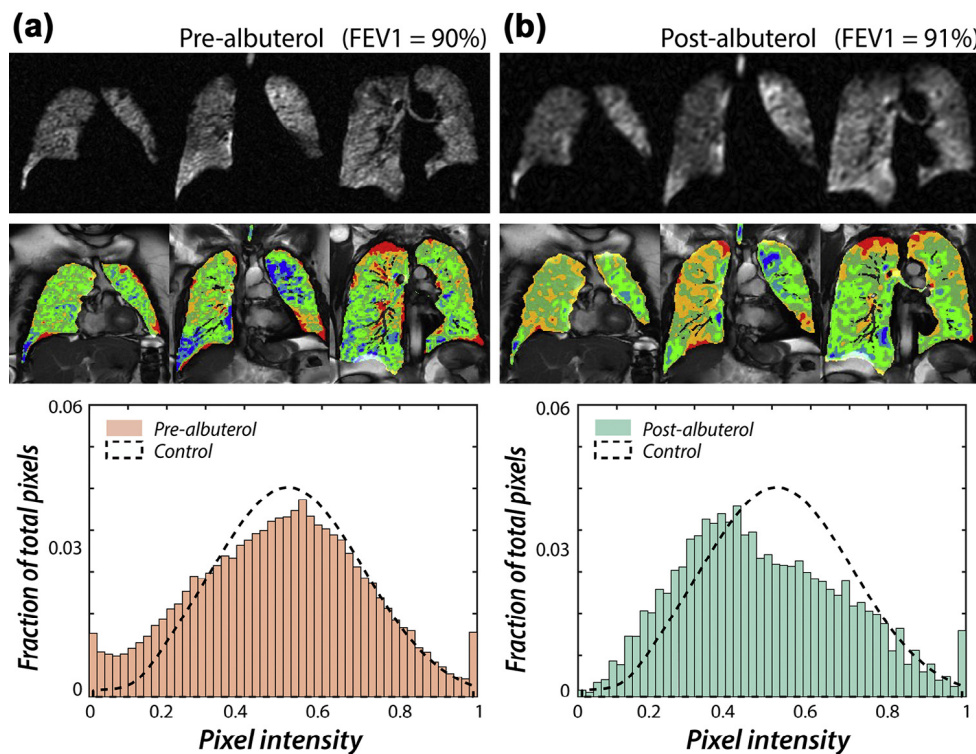


Figure 9. Ventilation distribution in a patient with mild intermittent asthma who did not respond to albuterol based on FEV1 criteria. **(a)** The binning map (top) and histogram (bottom) before albuterol treatment. **(b)** The binning map (top) and histogram (bottom) after albuterol treatment. The ventilation distribution histogram after albuterol treatment showed decreased VDR but increased LVR at the expense of normally ventilated regions. This may be the result of more normal airways dilating and redistributing ventilation.

The ¹²⁹Xe-derived ventilation distributions in younger and older asthmatics also exhibited a significantly different character. Although the greater fractions of VDR and LVR seen in older asthmatics are somewhat expected (47), a more striking finding was the significant reduction of HVR in the older vs younger patients. HVR may correspond to part of the gravity-dependent regions of the lung that naturally receive more ventilation or may represent regions of the lung that are subserved by collateral airways. Collateral ventilation is an important protective mechanism for minimizing ventilation-perfusion heterogeneity (48,49). It has been shown using the stop-flow maneuvers by Kaminsky et al. that asthma patients have more narrowing and closure of collateral airways and that closure was sensitive to challenge with cool-dry air (50). Thus, narrowing of these airways in the older asthmatic patients could explain our observed decrease in HVR. However, the exact pathophysiological relevance of VDR, LVR, and HVR require further validation in additional pulmonary phenotypes.

A third example demonstrating the sensitivity of ¹²⁹Xe MRI is given by its ability to detect ventilation abnormalities in mild asthmatics with normal spirometry. Normal spirometry in patients with mild intermittent asthma are not uncommon, indicating that this subgroup has fairly mild and well-controlled airway hyper-reactivity. In our study of 19 asthmatics, 12 were asymptomatic with mild intermittent disease and normal FEV1, and 6 exhibited significant ventilation defects.

Detecting such defects in asymptomatic individuals has a precedent in ³He MRI, where Altes et al. showed peripheral ventilation defects in 7 of 10 asthmatics whose FEV1 ranged from 62% to 126% predicted (23). Building on this, de Lange et al. used ³He to study 58 patients with asthma but found no difference in the ventilation defect score between patients with mild intermittent asthma and healthy subjects (18). It appears ¹²⁹Xe may be more sensitive to the entire ventilation distribution than ³He, and analyzing it in its entirety yields insights beyond VDP. Similarly, ¹²⁹Xe MRI revealed radically different ventilation distributions in patients with similarly low FEV1. This finding may indicate that the current categories of asthma could benefit from further stratification by ventilation distribution patterns. However, of the 12 mild intermittent asthmatics, 7 exhibited a ventilation distribution that was similar to our healthy reference cohort. This similarity and lack of obvious difference in quantitative metrics derived from the histogram pose difficulties in separating intermittent asthmatics from controls. Further studies will therefore be needed to find signatures that discriminate these subjects, as well as to assess the robustness of this analysis methodology and how well it correlates with other clinical phenotypes (51).

And finally, the sensitivity of ¹²⁹Xe MRI provides insights into the way the ventilation distribution changes in patients with mild intermittent asthma before and after albuterol treatment. In one asthmatic exhibiting a 15% improvement in FEV1

after albuterol treatment, ^{129}Xe MRI showed a ventilation distribution that shifted toward higher values, causing VDR and LVR to decrease and HVR to increase. These changes were consistent with bronchodilation at the narrowed (or more diseased) airways and thus moved the “choke point” downstream (toward the mouth) (52). Such reversibility of ventilation defects has been previously visualized by ^3He and ^{129}Xe MRI in asthma patients who responded to a bronchodilator (28,53,54). Unique to our study is the illustration of an asthmatic with normal baseline FEV₁ and no FEV₁ response after bronchodilator use, where ^{129}Xe MRI reveals a substantial redistribution of ventilation. In this case, VDR was reduced, but this reduction was accompanied by an increase in LVR, suggesting that bronchodilation may have also occurred in more normal (less affected) and distal airways. The changes, however, were insufficient to shift the choke point downstream (52). Thus, the ^{129}Xe MRI ventilation distribution may serve as a more sensitive end point for describing albuterol response than spirometry. ^{129}Xe MRI could also be used to investigate the mechanisms for therapeutic response in patients with obstructive airway pathology. Because the technique is inherently noninvasive, it is well suited to repeat application on any desired timescale. Changes in ventilation distribution without changes in spirometry have been demonstrated when ventilation heterogeneity was quantified by more sensitive techniques, such as MBNW (55) and MIGET (53). Moreover, LCI derived from the MBNW test is the earliest measurement for small airway dysfunction in cystic fibrosis (8,9,56); Macleod et al. (55) reported a significantly elevated LCI suggesting ventilation heterogeneity in asthmatic children compared to age-matched healthy children. So far, LCI has been primarily applied to pediatric populations (10,55) but could be the most appropriate metric against which to compare ^{129}Xe MRI in future studies.

In summary, the analysis of ^{129}Xe MRI scans by histogram rescaling and objectively generated six-bin maps represents a novel way to more comprehensively analyze the ventilation distribution and holds significant promise to more sensitively detect ventilation abnormalities under a variety of baseline conditions and stimuli. This analysis method has the sensitivity to detect regional changes in ventilation, even when spirometry does not. With additional, larger studies, this analysis methodology may prove broadly useful for a more sensitive regional assessment of obstructive lung disease and detection of therapeutic efficacy.

REFERENCES

- Wagner PD, Laravuso RB, Uhl RR, et al. Continuous distributions of ventilation-perfusion ratios in normal subjects breathing air and 100 per cent O₂. *J Clin Invest* 1974; 54:54–68.
- Lewis SM, Evans JW, Jalowayski AA. Continuous distributions of specific ventilation recovered from inert gas washout. *J Appl Physiol Respir Environ Exerc Physiol* 1978; 44:416–423.
- Simon BA, Kaczka DW, Bankier AA, et al. What can computed tomography and magnetic resonance imaging tell us about ventilation? *J Appl Physiol* 2012; 113:647–657.
- Tzeng YS, Lutchen K, Albert M. The difference in ventilation heterogeneity between asthmatic and healthy subjects quantified using hyperpolarized ^3He MRI. *J Appl Physiol* 2009; 106:813–822.
- Verbanck S, Thompson BR, Schuemans D, et al. Ventilation heterogeneity in the acinar and conductive zones of the normal ageing lung. *Thorax* 2012; 67:789–795.
- Wagner PD, Saltzman HA, West JB. Measurement of continuous distributions of ventilation-perfusion ratios: theory. *J Appl Physiol* 1974; 36:588–599.
- Robinson PD, Latzin P, Verbanck S, et al. Consensus statement for inert gas washout measurement using multiple- and single-breath tests. *Eur Respir J* 2013; 41:507–522.
- Horsley A, Wild JM. Ventilation heterogeneity and the benefits and challenges of multiple breath washout testing in patients with cystic fibrosis. *Paediatr Respir Rev* 2015; 16(suppl 1):15–18.
- Kent L, Reix P, Innes JA, et al. Lung clearance index: evidence for use in clinical trials in cystic fibrosis. *J Cyst Fibros* 2014; 13:123–138.
- Horsley A. Lung clearance index in the assessment of airways disease. *Respir Med* 2009; 103:793–799.
- Aurora P, Gustafsson P, Bush A, et al. Multiple breath inert gas washout as a measure of ventilation distribution in children with cystic fibrosis. *Thorax* 2004; 59:1068–1073.
- Edelman RR, Hatabu H, Tadamura E, et al. Noninvasive assessment of regional ventilation in the human lung using oxygen-enhanced magnetic resonance imaging. *Nat Med* 1996; 2:1236–1239.
- Ohno Y, Hatabu H, Takenaka D, et al. Dynamic oxygen-enhanced MRI reflects diffusing capacity of the lung. *Magn Reson Med* 2002; 47:1139–1144.
- Sa RC, Asadi AK, Theilmann RJ, et al. Validating the distribution of specific ventilation in healthy humans measured using proton MR imaging. *J Appl Physiol* 2014; 116:1048–1056.
- Halaweh AF, Moon RE, Foster WM, et al. Perfluoropropane gas as a magnetic resonance lung imaging contrast agent in humans. *Chest* 2013; 144:1300–1310.
- Ouriadov AV, Fox MS, Couch MJ, et al. In vivo regional ventilation mapping using fluorinated gas MRI with an x-centric FGRE method. *Magn Reson Med* 2015; 74:550–557.
- Salerno M, Altes TA, Mugler JP, 3rd, et al. Hyperpolarized noble gas MR imaging of the lung: potential clinical applications. *Eur J Radiol* 2001; 40:33–44.
- de Lange EE, Altes TA, Patrie JT, et al. Evaluation of asthma with hyperpolarized helium-3 MRI: correlation with clinical severity and spirometry. *Chest* 2006; 130:1055–1062.
- Costella S, Kirby M, Maksym GN, et al. Regional pulmonary response to a methacholine challenge using hyperpolarized ^3He magnetic resonance imaging. *Respirology* 2012; 17:1237–1246.
- Kirby M, Svenningsen S, Owragi A, et al. Hyperpolarized ^3He and ^{129}Xe MR imaging in healthy volunteers and patients with chronic obstructive pulmonary disease. *Radiology* 2012; 265:600–610.
- Svenningsen S, Kirby M, Starr D, et al. What are ventilation defects in asthma? *Thorax* 2014; 69:63–71.
- Fain SB, Gonzalez-Fernandez G, Peterson ET, et al. Evaluation of structure-function relationships in asthma using multidetector CT and hyperpolarized He-3 MRI. *Acad Radiol* 2008; 15:753–762.
- Altes TA, Powers PL, Knight-Scott J, et al. Hyperpolarized ^3He MR lung ventilation imaging in asthmatics: preliminary findings. *J Magn Reson Imaging* 2001; 13:378–384.
- Mugler JP, 3rd, Altes TA. Hyperpolarized ^{129}Xe MRI of the human lung. *J Magn Reson Imaging* 2013; 37:313–331.
- Virgincar RS, Cleveland ZI, Kaushik SS, et al. Quantitative analysis of hyperpolarized ^{129}Xe ventilation imaging in healthy volunteers and subjects with chronic obstructive pulmonary disease. *NMR Biomed* 2013; 26:424–435.
- Stewart NJ, Norquay G, Griffiths PD, et al. Feasibility of human lung ventilation imaging using highly polarized naturally abundant xenon and optimized three-dimensional steady-state free precession. *Magn Reson Med* 2015; 74:346–352.
- Kirby M, Svenningsen S, Kanhere N, et al. Pulmonary ventilation visualized using hyperpolarized helium-3 and xenon-129 magnetic resonance imaging: differences in COPD and relationship to emphysema. *J Appl Physiol* 2013; 114:707–715.
- Svenningsen S, Kirby M, Starr D, et al. Hyperpolarized ^3He and ^{129}Xe MRI: differences in asthma before bronchodilation. *J Magn Reson Imaging* 2013; 38:1521–1530.

29. Woodhouse N, Wild JM, Paley MN, et al. Combined helium-3/proton magnetic resonance imaging measurement of ventilated lung volumes in smokers compared to never-smokers. *J Magn Reson Imaging* 2005; 21:365–369.
30. Kirby M, Heydarian M, Svenningsen S, et al. Hyperpolarized ³He magnetic resonance functional imaging semiautomated segmentation. *Acad Radiol* 2012; 19:141–152.
31. He M, Kaushik SS, Robertson SH, et al. Extending semiautomatic ventilation defect analysis for hyperpolarized (¹²⁹Xe) ventilation MRI. *Acad Radiol* 2014; 21:1530–1541.
32. Hahn AD, Cadman RV, Sorkness RL, et al. Redistribution of inhaled hyperpolarized He³ gas during breath-hold differs by asthma severity. *J Appl Physiol* 2016; 120:526–536. Jap 00197 2015.
33. Ebner L, He M, Virginica RS, et al. Hyperpolarized ¹²⁹Xenon MRI to quantify regional ventilation differences in mild to moderate asthma: a prospective comparison between semi-automated ventilation defect percentage calculation and pulmonary function tests. *Invest Radiol* 2016; In Press.
34. He M, Robertson SH, Kaushik SS, et al. Dose and pulse sequence considerations for hyperpolarized (¹²⁹Xe) ventilation MRI. *Magn Reson Imaging* 2015; 33:877–885.
35. Fulambarker A, Copur AS, Javet A, et al. Reference values for pulmonary function in Asian Indians living in the United States. *Chest* 2004; 126:1225–1233.
36. Kirby M, Mathew L, Wheatley A, et al. Chronic obstructive pulmonary disease: longitudinal hyperpolarized ³He MR imaging. *Radiology* 2010; 256:280–289.
37. Hamerly G, Elkan C. Learning the K in K-means. *NIPS* 2003; 17.
38. MacKay DJC. Information theory, inference, and learning algorithms. Cambridge, UK, New York: Cambridge University Press, 2004. Reprinted with corrections. ed.
39. Deninger AJ, Mansson S, Petersson JS, et al. Quantitative measurement of regional lung ventilation using He-3 MRI. *Magn Reson Med* 2002; 48:223–232.
40. Emami K, Kadlecak SJ, Woodburn JM, et al. Improved technique for measurement of regional fractional ventilation by hyperpolarized ³He MRI. *Magn Reson Med* 2010; 63:137–150.
41. Horn FC, Deppe MH, Marshall H, et al. Quantification of regional fractional ventilation in human subjects by measurement of hyperpolarized ³He washout with 2D and 3D MRI. *J Appl Physiol* 2014; 116:129–139.
42. Hamedani H, Clapp JT, Kadlecak SJ, et al. Regional fractional ventilation by using multibreath wash-in ³He MR imaging. *Radiology* 2016; 279:917–924. 150495.
43. Sa RC, Cronin MV, Henderson AC, et al. Vertical distribution of specific ventilation in normal supine humans measured by oxygen-enhanced proton MRI. *J Appl Physiol* 2010; 109:1950–1959.
44. Sheikh K, Paulin GA, Svenningsen S, et al. Pulmonary ventilation defects in older never-smokers. *J Appl Physiol* 2014; 117:297–306.
45. Janssens JP, Pache JC, Nicod LP. Physiological changes in respiratory function associated with ageing. *Eur Respir J* 1999; 13:197–205.
46. Cardus J, Burgos F, Diaz O, et al. Increase in pulmonary ventilation-perfusion inequality with age in healthy individuals. *Am J Respir Crit Care Med* 1997; 156(2 Pt 1):648–653.
47. Heckscher T, Bass H, Oriol A, et al. Regional lung function in patients with bronchial asthma. *J Clin Invest* 1968; 47:1063–1070.
48. Gompelmann D, Eberhardt R, Herth FJ. Collateral ventilation. *Respiration* 2013; 85:515–520.
49. Macklem PT. Airway obstruction and collateral ventilation. *Physiol Rev* 1971; 51:368–436.
50. Kaminsky DA, Bates JH, Irvin CG. Effects of cool, dry air stimulation on peripheral lung mechanics in asthma. *Am J Respir Crit Care Med* 2000; 162:179–186.
51. Moore WC, Meyers DA, Wenzel SE, et al. Identification of asthma phenotypes using cluster analysis in the severe asthma research program. *Am J Respir Crit Care Med* 2010; 181:315–323.
52. Despas PJ, Leroux M, Macklem PT. Site of airway obstruction in asthma as determined by measuring maximal expiratory flow breathing air and a helium-oxygen mixture. *J Clin Invest* 1972; 51:3235–3243.
53. Lagerstrand L, Skedinger M, Ihre E, et al. Spirometry and ventilation-perfusion inequality in patients with mild allergic asthma before and during the pollen season. *Clin Physiol* 1995; 15:355–364.
54. Cardus J, Burgos F, Diaz O, et al. Increase in pulmonary ventilation-perfusion inequality with age in healthy individuals. *Am J Respir Crit Care Med* 1997; 156:648–653.
55. Macleod KA, Horsley AR, Bell NJ, et al. Ventilation heterogeneity in children with well controlled asthma with normal spirometry indicates residual airways disease. *Thorax* 2009; 64:33–37.
56. Kraemer R, Blum A, Schibler A, et al. Ventilation inhomogeneities in relation to standard lung function in patients with cystic fibrosis. *Am J Resp Crit Care* 2005; 171:371–378.